Pergamon

Int. J. Solids Structures Vol. 35, Nos 34–35, pp. 4895–4904, 1998

Printed in Great Britain
0020–7683/98/$—see front matter

PII : S0020–7683(98)00100–0

INDENTATION OF A SHARP PENETROMETER IN A POROELASTIC MEDIUM

DEREK ELSWORTH†
Department of Mineral Engineering, 104 Hosler Building, Pennsylvania State University, University Park, PA 16802-5000, U.S.A.

(*Received* 5 *May* 1997 ; *in revised form* 20 *January* 1998)

Abstract—Solution is developed for the build-up, steady and post-arrest dissipative pore fluid pressure fields that develop around a conical penetrometer advanced in a poroelastic medium. The analog with cone penetrometer testing is direct, and is used to enable continuous distributions of permeability and diffusivity to be determined, with depth. Solution for a point normal dislocation migrating in a poroelastic medium is extended to incorporate the influence of a tapered tip. Steady pressures develop relative to the migrating tip geometry with distribution conditioned by the non-dimensional penetration rate, U_D, incorporating penetration rate, hydraulic diffusivity and penetrometer radius. The near-spherical pressure distribution, recovered for low penetration velocities, becomes radial as penetration rate increases. Along the penetrometer shaft, non-dimensional induced pore fluid pressures, P_D, are independent of penetration rate, U_D, and asymptote to an inverse radial distribution remote from the tip as $P_D = 1/x_D$. This importantly identifies the control on penetration induced pore fluid pressure as the magnitude of permeability, embodied in the non-dimensional pressure, P_D, rather than a dependence on hydraulic diffusivity, as had previously been considered. Induced pore pressures are singular in the zone of tip taper for the assumed zero radius of the penetrometer, negating the direct evaluation of permeability magnitudes from pressures recorded on the cone face. However, the finite magnitudes of fluid pressures evaluated on the shaft may be correlated with field data to independently evaluate magnitudes of permeability during steady penetration.

1. INTRODUCTION

A variety of methods are available to characterize the stratigraphy of soils through the use of the cone penetrometer test. This test involves steady penetration of saturated soils by a 10 cm^2 end-bearing area cone, with a 60° interapical angle, at a standard rate of 2 cm/s. A continuous record of stratigraphy with depth is obtained by cross-correlating the indices of penetration induced pore fluid pressure, end-bearing and penetrometer sleeve friction. Empirical correlations (Robertson *et al*., 1986) provide methods of qualitatively defining soil types, with more quantitative methods available to evaluate magnitudes of critical parameters, including permeability, k, and hydraulic diffusivity, c. These methods of characterization all rely on the evaluation of penetration induced pore pressure in the near-tip process zone, subject to a variety of simplifying assumptions.

Analytical methods, developed for the evaluation of cone bearing and dissipation data, must be applied in the evaluation of transport properties. These methods may be conveniently divided between static and migrating models. This definition is chosen to represent whether the solution is able to represent the migration of the penetrometer tip within the penetrated solid, a feature that becomes increasingly important as partially drained behavior is represented.

Static models relate primarily to cavity expansion results for spherical (Ladanyi, 1963) and cylindrical (Randolph and Wroth, 1979) geometries, typically restricted to cohesive materials, but also capable of incorporating frictional behavior (Vesic, 1972) and shear induced pore pressures (Chen and Mayne, 1994). These results have been applied to define the initial undrained distributions of pore pressure and their subsequent dissipation (Torstensson, 1977 ; Randolph and Wroth, 1979 ; Chen and Mayne, 1994), and used exclusively in the determination of hydraulic diffusivity, c_h or c_v, in the horizontal or vertical plane.

† Tel. : 001 814 863-1643. Fax : 001 814 865-3248. E-mail : elsworth@pnge.psu.edu.

Despite the capability to accommodate a variety of complex material models, cavity expansion results represent only static behavior and are incapable of reproducing refined strain or pore pressure fields that result at the cone tip. The limitation to static problems is not severe since the twin geometries of spherical and cylindrical cavity expansion represent bounding geometries of slow and fast penetration, respectively. The terms "slow" and "fast" are relative, but may be indexed to hydraulic diffusivity, with "slow" representing the case where penetration is slow in comparison to the rate of pressure dissipation.

The more pressing limitation in the use of cavity expansion models, is the inability to accommodate the precise tip geometry of the penetrometer. Penetration generated pore pressure magnitudes have been shown strongly dependent on tip shape and degree of taper (Levadoux and Baligh, 1986), and relative position of the pressure sensing element locations (Robertson *et al*., 1992). The inability of cavity expansion methods to adequately represent these facets makes their direct application to data reduction problematic.

Furthermore, application of static models are restricted to the determination of hydraulic diffusivity, c, using correlations with pressure dissipation rate as an appropriate index. Attempted correlations between hydraulic conductivity, k, and pressure dissipation rate have been attempted (Schmertmann, 1978), but have been unable to provide substantiated results (Robertson *et al*., 1992). There is no clear reason why hydraulic conductivity should be related to dissipation time, since the transient dissipation process is moderated by magnitudes of hydraulic diffusivity, alone.

Migrating models are those that accommodate the non-inertial dynamic effects of the moving penetrometer tip. Of critical importance remain the two issues of (i) accurately determining the evolving strain field, local to the tip, and (ii) accommodating partial drainage conditions by enabling concurrent generation and dissipation of pore-pressures. These requirements are met, to varying degrees, in different models.

The evolving strain field may be determined from consideration of kinematic failure mechanisms, either disregarding (Baligh and Scott, 1976) or including (Drescher and Kang, 1987) self weight, and from consideration of steady plastic flow (Tumay *et al*., 1985; Acar and Tumay, 1986). Instantaneous pore pressure distributions may be recovered through use of appropriate pore pressure parameters (Skempton, 1954; Biot and Willis, 1957). Many of the complexities involved in accurately defining the strain field through rigorous mechanical analyses may be circumvented by adopting the concept of strain path analysis (Baligh, 1985). In this, subtle variations in strain distribution that may occur around the penetrating tip are assumed of secondary importance to the intense impacts of material nonlinearity. Correspondingly, an approximate solution is sought to the mechanical problem, neglecting rigorous solution of the equilibrium equations, but providing a robust evaluation of strain distributions to the applied displacement (or displacement-rate) boundary conditions. This procedure is shown to provide adequate predictions of undrained pore pressure generation (Levadoux and Baligh, 1986; Baligh and Levadoux, 1986), adequately incorporating cone geometry effects, and may be applied equally to complex and relatively straightforward (Teh and Houlsby, 1991) material models.

Although arbitrarily complex material models may be applied to strain path type methods, those employing simple failure criteria, such as the undrained von Mises criterion (Teh and Houlsby, 1991) are particularly appealing. Undrained post-penetration pore pressures may be readily evaluated and their dissipation monitored. Of importance in these analyses, is to note that dissipation behavior is only weakly conditioned by the soil rigidity, and that coefficient of consolidation, c, may be determined. Independent evaluation of hydraulic conductivity, from the same sounding data, requires further knowledge of the shear modulus of the soil, G. This cannot be determined independently from the dissipative data.

An alternative to using strain-path methods, that currently allow only undrained behavior to be evaluated, is to use dislocation based methods (Elsworth, 1991; Elsworth, 1992). These methods enable both undrained and partially drained behavior to be accommodated, with concurrent generation and dissipation of pore fluid pressure straightforwardly incorporated. They also offer the advantage that coherent parameters, representing the full spectrum of undrained and partially drained behaviors, are also utilized.

The main limitations are that general pseudo-elastic material (poroelastic) behavior is used, negating the development of a true process zone at the penetrometer tip, and that the current analyses are for moving point dislocations within linear poroelastic media, that do not adequately represent the influence of the tip geometry on pressure generation. Despite these limitations, the distribution of penetration-induced pore fluid pressures evaluated from the dislocation analysis closely matches undrained behavior observed (Baligh and Levadoux, 1986) and replicated by other methods (Levadoux and Baligh, 1986; Teh and Houlsby, 1991) and are not restricted to undrained behavior, alone.

Magnitudes of pre-arrest pore fluid pressures are conditioned by the "strength" of the point dislocation, suggesting that cone end-bearing may be evaluated, and correlated with the penetration induced pore pressure to enable hydraulic conductivity magnitudes to be recovered from the recorded distribution of peak (pre-arrest) pore pressure magnitudes.

This analysis may be extended to include the local geometry of the penetrometer tip by using a distribution of volumetric dislocations that closely approximate the geometry of tip advance. This is completed in the following.

2. DISLOCATION ANALYSIS

The behavior of a sharp penetrometer, moving within a poroelastic medium, may be represented by a moving volumetric dislocation of appropriate taper. The incremental form of this is a point volumetric dislocation, of volume $\mathrm{d}V$ (L^3), representing the dilatation in unit time, t, subjected to a volumetric dilation rate, v (L^3T^{-1}), as $\mathrm{d}V = v\,\mathrm{d}t$. For $t \geqslant 0$ a volumetric dislocation is introduced at the origin ($x = y = z = 0$) with the poroelastic medium moving at velocity $+U$ in the x-direction of the fixed Cartesian coordinate system, representing a dislocation migrating within an infinite medium, as illustrated in Fig. 1. The position of a point located at (x, y, z) at time t, would have been $((x-U(t-\tau)), y, z)$ at time τ. This migrating coordinate system enables the behavior for a static dislocation (Cleary, 1977; Elsworth, 1991) to be defined as

$$p - p_s = \frac{c\,\mathrm{d}V}{4\pi\bar{R}^3}\frac{\mu}{k}\frac{\bar{\xi}^3}{2\sqrt{\pi}}\mathrm{e}^{-(\bar{\xi}^2/4)} \tag{1}$$

with $\bar{\xi} = \bar{R}/\sqrt{c(t-\tau)}$ and $\bar{R}^2 = [x-U(t-\tau)]^2 + y^2 + z^2$. The material properties defining the medium represent absolute pore fluid pressure, p, relative to the initial static fluid pressure, p_s, permeability, k, hydraulic diffusivity, c and dynamic viscosity of the fluid, μ. Substituting into eqn (1) for the incremental rate of dilatation as $\mathrm{d}V = v\,\mathrm{d}\tau$, and integrating in time yields after some rearrangement,

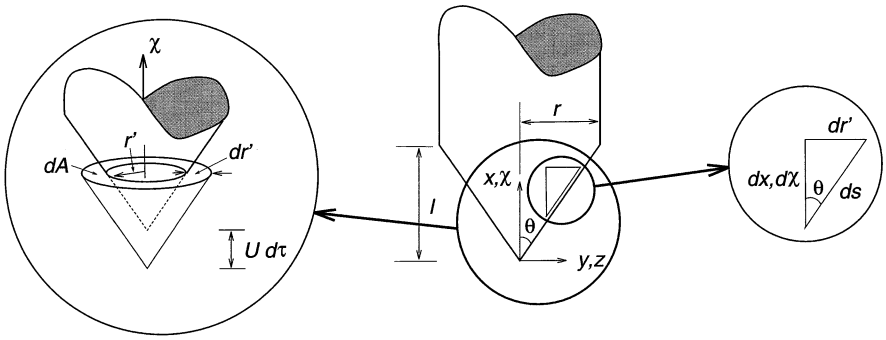

Fig. 1. Geometry of cone tip (center) definining length of taper, l, semi-apical angle, θ, and shaft radius, r. Coordinate system is attached to the cone apex and migrates with the penetrometer at velocity, U, in the direction of the negative x- or χ-axis. Incremental advance of length $U\,\mathrm{d}\tau$ in time $\mathrm{d}\tau$ results in expansion of a cavity (left), defined in magnitude by eqn (4).

$$p-p_s = \int_0^t \frac{cv}{4\pi \bar{R}^3} \frac{\mu}{k} \frac{\bar{\xi}^3}{2\sqrt{\pi}} e^{-(\bar{\xi}^2/4)} d\tau, \tag{2}$$

where v is the rate of volume change (L^3T^{-1}).

The substitution $\eta = R/2\sqrt{c(t-\tau)}$ may be used with $R = \sqrt{x^2+y^2+z^2}$, attached to the migrating coordinate system. Substituting these equalities into eqn (2) yields,

$$p-p_s = \frac{\mu}{k} \frac{v}{2\sqrt{\pi^3}R} e^{(Ux/2c)} \int_{R/2\sqrt{ct}}^{\infty} e^{-\eta^2-(UR/4c\eta)^2} d\eta. \tag{3}$$

This is the standard result reported (Elsworth, 1991) for a blunt penetrometer. To determine the form of the fluid pressure field that develops around a sharp penetrometer, tapered along its axis, the response for a point volumetric dislocation must be distributed to represent the taper of the moving feature. Consider the conical tip of a penetrometer of radius, r, as illustrated in Fig. 1, where the semi-apical angle, θ, and length of taper, l, define the geometry. A surrogate variable, χ is selected that parallels the x-axis, that may be used for integrating an appropriately weighted distribution of the point dislocations. Correspondingly, the projected area, dA, of a circumferential contour on the y-, z-plane is defined

$$dA = 2\pi r' dr' \begin{cases} r' = \chi \tan\theta \\ dr' = d\chi \tan\theta \end{cases} \tag{4}$$

which upon substitution of the components of eqn (4) yields

$$dA = 2\pi \tan^2\theta \chi \, d\chi. \tag{5}$$

For an incremental advance of the penetrometer of $U\,d\tau$ in time $d\tau$, the distribution of volume is $dV = dAU\,d\tau$, and substituting the relation of eqn (5), and noting from the previous that $dV = v\,d\tau$, then,

$$v = 2\pi \tan^2\theta U \chi \, d\chi. \tag{6}$$

This may be substituted directly into eqn (3) to yield,

$$p-p_s = \frac{\mu}{k} \frac{\tan^2\theta U}{\sqrt{\pi}} \int_0^l \frac{\chi}{\tilde{R}} e^{(U\tilde{x}/2c)} \int_{\tilde{R}/2\sqrt{ct}}^{\infty} e^{-\tilde{\eta}^2-(U\tilde{R}/4c\tilde{\eta})^2} d\tilde{\eta}\, d\chi \tag{7}$$

where the tilde overbar denotes inclusion of the variable coordinate of integration as $\tilde{x} = x-\chi$ and

$$\tilde{R} = \sqrt{\tilde{x}^2+y^2+z^2}$$
$$\tilde{\eta} = \frac{\tilde{R}}{\sqrt{4c(t-\tau)}} \tag{8}$$

representing migrating coordinates and a reciprocal non-dimensional time.

2.1. *Non-dimensional parameters*

The behavior of the system may be defined in terms of the non-dimensional parameters of excess fluid pressure, P_D, penetration rate, U_D, and time, t_D, as

$$P_D = \frac{4(p-p_s)}{Ur}\frac{k}{\mu} \tag{9}$$

$$U_D = \frac{Ur}{2c} \tag{10}$$

$$t_D = \frac{4ct}{r^2} \tag{11}$$

$$(x_D\,;y_D\,;z_D) = \frac{1}{r}(x\,;y\,;z) \tag{12}$$

with $\tilde{R}_D = \sqrt{\tilde{x}_D^2+y_D^2+z_D^2}$, $\tilde{x}_D = \tilde{x}/r$ or $\tilde{x}_D = x_D-\chi_D$. These may be substituted into eqn (7) to give, in final form the behavior around a tapered penetrometer with tip length, $l_D = l/r$ as

$$P_D = \frac{4\tan^2\theta}{\sqrt{\pi}}\int_0^{l_D}\frac{\chi_D}{\tilde{R}_D}\mathrm{e}^{U_D\tilde{x}_D}\int_{\tilde{R}_D/\sqrt{t_D}}^{\infty}\mathrm{e}^{-\tilde{\eta}^2-(U_D\tilde{R}_D/2\tilde{\eta})^2}\,\mathrm{d}\tilde{\eta}\,\mathrm{d}\chi_D. \tag{13}$$

This enables magnitudes of pore pressure build-up to be determined following initiation of penetration within an infinite medium. Application to this is described in the following.

3. PARAMETRIC BEHAVIOR

3.1. *Steady penetration*

In the limit as $t_D \to \infty$, the lower limit of integration of eqn (13), approaches zero, enabling simplification as,

$$P_D = 2\tan^2\theta\int_0^{l_D}\frac{\chi_D}{\tilde{R}_D}\mathrm{e}^{-U_D(\tilde{R}_D-\tilde{x}_D)}\,\mathrm{d}\chi_D. \tag{14}$$

This is the steady solution where the pore fluid pressure remains constant around the tip of the penetrometer when viewed relative to the migrating coordinate system. Remote from the penetrometer tip ($\tilde{R}_D \to \infty$) the integral may be decoupled to evaluate $2\tan^2\theta$ $\int_0^{l_D}\chi_D\,\mathrm{d}\chi_D = \tan^2\theta l_D^2 = 1$ and the form of eqn (14) reduces to the form for a point moving dislocation located at the origin of the moving coordinate system as,

$$P_D = \frac{1}{R_D}\mathrm{e}^{-U_D(R_D-x_D)}. \tag{15}$$

This is the same result as for a blunt penetrometer (Elsworth, 1991 ; Elsworth, 1992). The integral of eqn (14) may be simplified by considering the portion on the χ-axis representing the axis of the penetrometer, with $y = z = 0$. Behind the shoulder of the conical penetrometer ($x_D \geqslant l_D$) the solution simplifies to

$$\frac{P_D}{2\tan^2\theta} = \int_0^{l_D}\frac{\chi_D}{x_D-\chi_D}\mathrm{d}\chi_D = -x_D\ln[\chi_D-x_D]-\chi_D\big|_0^{l_D} \quad (x_D \geqslant l_D) \tag{16}$$

and ahead of the penetrometer tip ($x_D \leqslant 0$),

$$\frac{P_D}{2\tan^2\theta} = \int_0^{l_D} -\frac{\chi_D}{x_D-\chi_D} e^{+2U_D(x_D-\chi_D)}\,d\chi_D$$

$$= x_D E_i[2U_D(x_D-\chi_D)] - \frac{1}{2U_D} e^{2U_D(x_D-\chi_D)}\Big|_0^{l_D} \quad (x_D \leqslant 0). \tag{17}$$

In this the exponential integral, $E_i[z]$, is defined as $E_i[z] = -\int_{-z}^{\infty}(e^{-t}/t)\,dt$ (Abramowitz and Stegun, 1970). On the shaft, pore fluid pressures are not influenced by penetration rate, U_D, but asymptote to the assumed $1/x_D$ distribution for a moving point dislocation. Ahead of the tip, contours of induced pressure are strongly compressed with increasing U_D, and maintain a spherical distribution for low penetration rates, $U_D \leqslant 10^0$.

The magnitude of P_D may also be determined in the range $0 \leqslant x_D \leqslant l_D$ by adding eqns (16) and (17) with the upper limit of eqn (16) and the lower limit of eqn (17) both set to x_D. Using the substitution $E_i[z] = \gamma + \ln[z] + \Sigma(z^n/nn!)$, pore pressures, P_D, are singular in this range, due to the assumed zero radius of the conical tip of the cone. In this, γ is Euler's constant, defined as $\gamma = 0.5772156647$.

The distributions of steady pore fluid pressures developed around the tip are illustrated in Fig. 2 for a 120° cone ($2\theta = 120°$) with the tip centered on the origin, using eqn (14). Bounding behaviors are apparent in the far-field representing spherical symmetry for low penetration rates ($U_D \to 0$) and approaching radial symmetry at high penetration rates. This results from the general correspondence to eqn (15) in the far-field as the local influence of the distributed dislocation diminishes. As non-dimensional penetration rate, U_D,

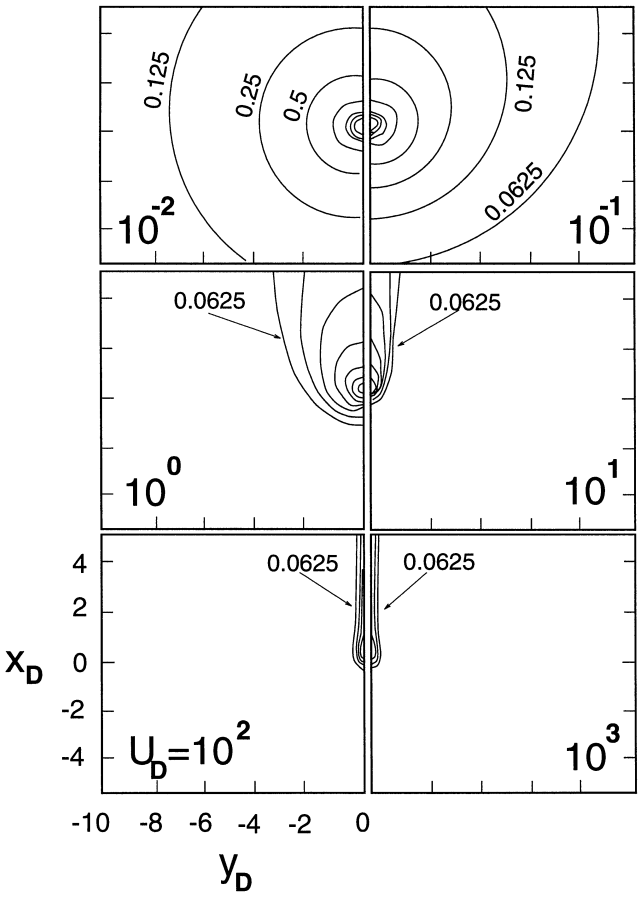

Fig. 2. Steady pressure distribution centered on the tip of a 120° (2θ) cone. Taper length is defined by semi-apical angle as $l_D = 1/\tan\theta$. Results document magnitudes of P_D in multiples of 2^{-n} within a radius of $R_D = 5$ of the cone tip.

increases the developing pressure bulb shrinks around the penetrometer tip. If local behavior is considered around the tip, again using eqn (14), the pressure distribution sheds the main components of spherical or radial symmetry. Tip-local pore pressures asymptote to a local form for $U_D > 10^\circ$ but not at the other end of the spectrum, as $U_D \to \infty$. This similar behavior is seen for a blunt penetrometer, where self-similar profiles are observed in changing scale, as indexed by the non-dimensional penetration rate. For the blunt penetrometer (Elsworth, 1991), reducing the length scale of observation by two orders of magnitude raises pressure magnitudes, P_D, by two orders of magnitude and indexes the distribution to that at the larger scale but transposed by a U_D magnitude two orders of magnitude higher. This is apparent from the dependence of the pore fluid pressure distribution on the parameter groupings of $U_D x_D$ and $U_D R_D$, in eqn (15).

The distribution of pore fluid pressure along the shaft may also be evaluated, as illustrated in Fig. 3. In the zone ahead of the shoulder of the penetrometer ($0 < x_D < l_D$), the pore fluid pressure magnitudes are singular, due to the assumed zero radius of the penetrometer. Behind this shoulder, the asymptotic magnitudes are defined by eqn (16), which upon substitution of the limits yields

$$P_D = 2\tan^2\theta\, x_D\left[\ln\left[\frac{x_D}{x_D - l_D}\right] - \frac{l_D}{x_D}\right] \tag{18}$$

on the shaft. This steady behavior reduces to $P_D = 1/x_D$ for large x_D, identical to the behavior for a blunt penetrometer. The $1/x_D$ distribution along the shaft is valid only at large separations from the tip, where the behavior for the tapered penetrometer approaches that for the blunt penetrometer for x_D greater than a few taper lengths, l_D. This is dependent only on the choice of taper angle for the cone, θ, as $\tan\theta = 1/l_D$. Usefully, along the shaft, pore pressures are only a function of location, penetrometer taper and dimensionless pressure, P_D. Correspondingly, P_D includes permeability, k, but not diffusivity, c, suggesting that shaft pressures are a function of permeability, alone, enabling permeability profiles to be extracted from steady penetration data. This has important implications since permeability magnitudes may be determined on-the-fly, without requiring penetrometer arrest and pressure dissipation, as typically needed in determining diffusivity magnitudes.

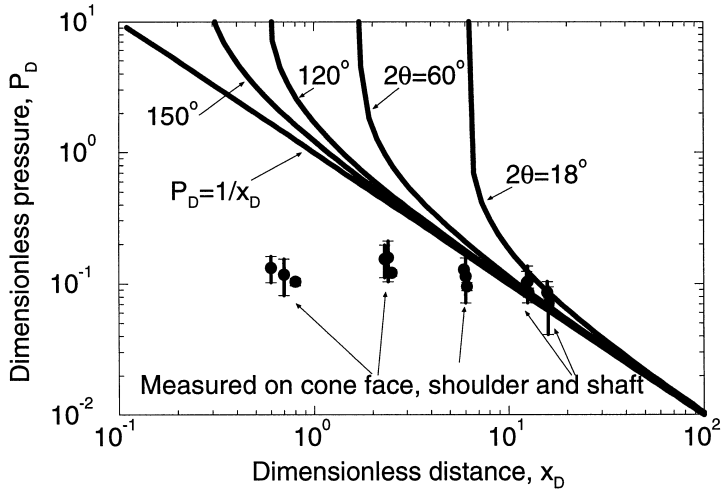

Fig. 3. Steady distribution of pore fluid pressure along the penetrometer shaft illustrating the influence of penetrometer taper relative to the behavior for a blunt penetrometer. Data are for penetration of an 18° cone in Boston Blue Clay (Baligh and Levadoux, 1986) at depths of between 13 and 26 m. Note that the majority of data are on the cone face or shoulder, where the solution is singular as a result of the assumed zero-radius dislocation.

3.2. *Post-arrest*

Behavior, post-arrest may be evaluated by superposing a moving dislocation of negative strength, beginning at the time of arrest, $t'_D = 4ct'/r^2$, over the non-arrested moving dislocation. Behavior at any time, $t_D > t'_D$, may be determined from the coincident and colinear moving dislocations, the first representing dilatation from $0 \rightarrow t_D$ and the second representing a contractile volumetric dislocation from $t'_D \rightarrow t_D$. The system equations follow directly from eqn (13) as,

$$P_D = \frac{4\tan^2\theta}{\sqrt{\pi}} \int_0^{t_D} \frac{\chi_D}{\tilde{R}_D} e^{U_D \tilde{x}_D} \int_{\tilde{R}_D/\sqrt{t_D - t'_D}}^{\tilde{R}_D/\sqrt{t_D}} e^{-\tilde{\eta}^2 - (U_D \tilde{R}_D/2\tilde{\eta})^2} \, d\tilde{\eta} \, d\chi_D. \tag{19}$$

where the coordinate system migrates with the continuously migrating dislocation, post-arrest, and pressures are referenced relative to this coordinate system. To transform to coordinates relative to the arrested penetrometer, a linear transformation must be applied. Where the coordinate system $[\hat{x}, \hat{y}, \hat{z}]$ is chosen to represent locations relative to the arrested penetrometer, the linkage between the two coordinate systems is

$$\begin{aligned} x &= \hat{x} - U(t - t') \\ y &= \hat{y} \\ z &= \hat{z} \end{aligned} \tag{20}$$

where

$$\tilde{x} = \hat{x} - \chi = \hat{x} - U(t - t') - \chi. \tag{21}$$

The same non-dimensional coordinate system may be invoked, to yield the coordinate transform

$$x_D = \hat{x}_D - \tfrac{1}{2} U_D (t_D - t'_D) \tag{22}$$

and enable eqn (19) to be directly evaluated.

4. ON-THE-FLY PERMEABILITY EVALUATIONS

The observation that peak shaft pore pressure magnitudes are dependent only on permeability, penetration rate and penetrometer geometry suggest that permeability magnitudes may be recovered from shaft data. If absolute steady pressure magnitudes are available at a single location, permeability may be evaluated directly from eqn (18), noting the definition of P_D from eqn (9). If the differential pressure, $\Delta p = p_1 - p_2$, is recorded between two locations on the shaft, defined as x_1 and x_2, then magnitudes of permeability, k, or hydraulic conductivity, K, may be directly determined. Evaluating the differential in dimensionless pressures for the two locations, as $P_{D_1} - P_{D_2}$, yields, following some rearrangement,

$$\frac{K}{\rho g} = \frac{k}{\mu} = \frac{U x_1 \tan^2\theta}{2(p_1 - p_2)} \ln\left[\frac{x_1 (x_2 - l)^a}{x_2^a (x_1 - l)}\right]; \quad a = \frac{x_2}{x_1}; \quad l = \frac{r}{\tan\theta} \tag{23}$$

where ρ is density of the saturating fluid and g is gravitational acceleration. A required assumption is that the spatial differential in penetration-induced pore fluid pressures is much larger than the spatial differential in static pressures, hence $p_{s_1} \approx p_{s_2}$. For large x_D, this reduces to the behavior for a blunt penetrometer, as

$$\frac{K}{\rho g} = \frac{k}{\mu} = \frac{Ur^2}{4(p_1 - p_2)}\left[\frac{1}{x_1} - \frac{1}{x_2}\right]. \tag{24}$$

The advantage of using differential pressure is that the initial magnitude of static "formation" pressure, p_s, is sensibly not required. This obviates the need to determine the initial *in situ* fluid pressure profile. This simplification is not possible if a single shaft measuring location is used, requiring that full fluid pressure dissipation is followed (to background) on penetration arrest. The relative advantage is clear.

Applying eqn (23) to the shaft recorded data in Fig. 3 (Baligh and Levadoux, 1986) enables hydraulic conductivities, K, to be calculated directly for depths of 13.5 m (45 ft) and 25.5 m (85 ft). The data are for penetration in Boston Blue Clay with an 18° cone, of 10 cm^2 cross-section, at a standard penetration rate of 2 cm/s. Using the pressure differentials in the shaft data of Fig. 3, hydraulic conductivity may be recovered as $K = 2 \times 10^{-5}$ (13.5 m) to 1×10^{-5} (25.5 m) cm/s compared with field scale dissipation data in the range 2×10^{-6} (13.5 m maximum) to 2×10^{-8} (25.5 m minimum) cm/s. The shaft evaluated results are close to the measured magnitudes, but higher than the absolute range. This mismatch may result from a variety of sources, including measuring system compressibility, fluid pressure dissipation along the shaft–soil interface or nonlinearities in soil behavior. It is not clear from the data which of these effects may be predominant.

5. CONCLUSIONS

Solutions have been developed for the problem of a sharp penetrometer moving within a porous elastic medium where the influence of penetrometer motion is of critical importance. This solution provides an alternative in the reduction of cone penetrometer data, where typical approaches have been to consider the penetration process as either "stationary" of "undrained". In the former, the important concept of the porous medium "advecting" past the penetrometer tip is not incorporated. In the latter, the concurrent processes of pore pressure generation and diffusive dissipation are neglected. These dual components are important in representing behavior in "partially drained" penetration of sands and silts, and directly influence the ability to provide continuous profiles of transport parameters, including permeability magnitudes. It is shown that the resulting magnitudes of induced pore fluid pressures, and their distribution around the penetrometer tip, are strongly influenced by the non-dimensional rate of penetration, U_D. The influence of partial drainage cannot easily be neglected.

From the analysis, a minimum set of parameters define non-dimensional induced pressure, P_D, in the groupings of non-dimensional coordinates, (x_D, y_D, z_D), diffusive time, t_D, and penetration rate, U_D. These parameters are of use in describing behavior represented in these analyses, but also in characterizing the response of "non-ideal" systems of fluid saturated porous media that may involve both geometric and material nonlinearities. The ability to incorporate these effects would negate any semi-analytical treatment exposed here, but general trends in behavior are expected to be robust. The ability of the analytical models to provide a validation tool in deriving anticipated partially drained response is important.

The assumed zero radius of the penetrometer in the zone of tip taper results in singular magnitudes of induced pore pressure in this region ($0 \leqslant x_D \leqslant l_D; y_D = z_D = 0$). This is an artifact of the analysis. Behind the penetrometer tip, pore pressures asymptote to the blunt-penetrometer distribution of $P_D = 1/x_D$ as x_D becomes large. This distribution enables permeability magnitudes to be recovered from records of steady pressures recorded on the shaft. If data are available for a single monitoring location, permeability magnitudes may theoretically be recovered if the pre-penetration "formation" pressure, p_s is available, through application in eqn (18). Alternately, if two monitoring ports are available at different shaft locations, $x_1 \neq x_2$, then permeability magnitudes may be recovered from straightforward application of eqn (23). This correctly defines the functional relationships

that control the generation of the steady pressure distribution around a moving penetrometer, where the key controlling transport parameter is permeability, k, rather than hydraulic diffusivity, c. Correspondingly, correlations that use post-arrest dissipation rate to evaluate permeability are flawed since this behavior is controlled by diffusivity, c, and is independent of permeability magnitude. This outcome is positive since permeabilities derived from steady pore pressure magnitudes are intrinsically simpler to obtain than through use of time consuming pressure dissipation tests that rationally define magnitudes of diffusivity, alone.

Acknowledgements—The support of the National Science Foundation under grant CMS-9218547 is gratefully acknowledged. Two anonymous reviewers provided helpful comments in improving the manuscript.

REFERENCES

Abramowitz, M. and Stegun, I. A. (1970) *Handbook of Mathematical Functions with Formulas, Graphs, and Mathematical Tables*. Government Printing Office, Washington, D.C.

Acar, Y. and Tumay, M. T. (1986) Strain field around cones in steady penetration. *Journal of the Geotechnical Engineering Division, ASCE* **112**(2), 207–213.

Baligh, M. M. (1985) Strain path method. *Journal of the Geotechnical Engineering Division, ASCE* **111**(9), 1108–1136.

Baligh, M. M. and Levadoux, J. N. (1986) Consolidation after undrained piezocone penetration. II : Interpretation. *Journal of the Geotechnical Engineering Division, ASCE* **112**(7), 727–745.

Baligh, M. M. and Scott, R. F. (1976) Analysis of deep wedge penetration in clay. *Géotechnique* **26**(1), 185–208.

Biot, M. A. and Willis, D. G. (1957) The elastic coefficients of the theory of consolidation. *Journal of Applied Mechanics* **24,** 594–601.

Chen, Y. and Mayne, P. W. (1994).

Cleary, M. P. (1977) Fundamental solutions for a fluid saturated porous solid. *International Journal of Solids and Structures* **13**(9), 785–806.

Drescher, A. and Kang, M. (1987) Kinematic approach to limit load for steady penetration in rigid-plastic soils. *Géotechnique* **37**(3), 233–246.

Elsworth, D. (1991) Dislocation analysis of penetration in saturated porous media. *Journal of the Engineering Mechanics Division, ASCE* **117**(2), 391–408.

Elsworth, D. (1992) Pore pressure response due to penetration through layered media. *International Journal of Numerical and Analytical Methods in Geomechanics* **16**(1), 45–64.

Ladanyi, B. (1963) Expansion of a cavity in a saturated clay medium. *Journal of the Soil Mechanics and Foundation Engineering Division, ASCE* **89**(4), 127–161.

Levadoux, J. N. and Baligh, M. M. (1986) Consolidation after undrained piezocone penetration. I : Prediction. *Journal of the Geotechnical Engineering Division ASCE*, **112**(7), 707–726.

Randolph, M. and Wroth, C. (1979) An analytical solution for the consolidation around a driven pile. *International Journal of Numerical and Analytical Methods in Geomechanics* **3,** 217–229.

Robertson, P., Campanella, R., Gillespie, D. and Greig, J. (1986) Use of piezometer cone data. In *Proceedings of In Situ '86, American Society of Civil Engineers Speciality Conference GSP* 6, pp. 1263–1280, New York.

Robertson, P., Sully, J., Woeller, D., Lunne, T., Powell, J. M. and Gillespie, D. (1992) Estimating coefficient of consolidation from piezocone tests. *Canadian Geotechnical Journal* **29**(4), 539–550.

Schmertmann, J. H. (1978) Guidelines for cone penetration test, performance and design. Technical Report FHWA-78-209, Federal Highway Administration.

Skempton, A. W. (1954) The pore pressure coefficients A and B. *Géotechnique* **4**(4), 143–147.

Teh, C. and Houlsby, G. (1991) An analytical study of the cone penetration test in clay. *Géotechnique* **41,** 17–34.

Torstensson, B. A. (1977) The pore pressure probe. *Nordiske Geotekniske Mote* **34,** 34.1–34.15.

Tumay, M. T., Acar, Y. B., Cekirge, M. H. and Ramesh, N. (1985) Flow field around cone in steady penetration. *Journal of the Geotechnical Engineering Division, ASCE* **111**(2), 193–204.

Vesic, A. (1972) Expansion of cavities in infinite soil mass. *Journal of the Soil Mechanics and Foundation Engineering Division, ASCE* **98,** 265–290.